Performance of a novel sampling electromagnetic calorimeter with binary readout

J. A. Ballin[a], J. P. Crooks[b], P. D. Dauncey*[,a], A.-M. Magnan[a], Y. Mikami[c], O. D. Miller[c], M. Noy[a], V. Rajovic[c], M. M. Stanitzki[b], K. D. Stefanov[b], R. Turchetta[b], M. Tyndel[b], E. G. Villani[b], N. Watson[c], J. A. Wilson[c]

[a] *Department of Physics, Blackett Laboratory, Imperial College London, London, United Kingdom.*
[b] *STFC, Rutherford Appleton Laboratory, Chilton, Didcot, United Kingdom.*
[c] *School of Physics and Astronomy, University of Birmingham, Birmingham, United Kingdom.*

Abstract

We present a study of a novel concept for a sampling electromagnetic calorimeter. Using binary readout with very small pixels, then an estimate of the number of charged particles can be made. This is shown to give potentially better resolution than a more standard analogue readout of the deposited energy. The expected resolution of a full size binary calorimeter is presented, based on realistic assumptions of detector performance.

Key words: electromagnetic calorimetry
PACS: 12.34

1. Introduction and motivation

In this paper, we present results from a study of a novel approach to electromagnetic calorimeters (ECAL). In this approach, the readout of the ECAL is binary, meaning that each channel returns a yes/no result with no further amplitude information.

Although the potential applications for a binary ECAL are wide, the sensor discussed in this paper was designed for a specific application, namely the International Linear Collider (ILC) [1]. This is widely assumed to be the next worldwide particle physics frontier accelerator and it has a wide and rich physics programme [2, 3]. The work presented in this paper has been done within the context of the CALICE Collaboration [4], which is studying calorimetry for the ILC.

Many of the ILC physics measurements require reconstruction of heavy particles decaying into hadrons. To identify the decaying particles through the invariant mass of the hadronic jets requires excellent hadronic jet energy resolution. The main techniques which should be able to provide this resolution are based on Particle Flow Algorithms (PFA) [5, 6, 7], which require very high granularity calorimetry to allow the separation of the showers into the individual particles in the jet. For the ECALs, it is widely accepted that a sampling calorimeter will provide the best PFA performance, due to having good transverse and longitudinal granularity. The current state-of-the-art has silicon sensors as the detecting layers and tungsten as the converter and this structure is being considered by both the major ILC detector concepts [8, 9].

An electron, positron or photon interacting in material produces an electromagnetic (EM) shower containing a large number of charged particles and photons. A sampling EM calorimeter (ECAL) measures the charged particle component of the shower at various positions in the shower depth by having sensitive layers interspersed with a dense material which efficiently produces the shower. The sensitive layers operate by measuring the ionisation created by the charged particles in these layers and nor-

*Corresponding author
Email address: P.Dauncey@imperial.ac.uk (P. D. Dauncey)

mally the shower energy is estimated by measuring the energy deposited through the ionisation.

In this paper, we present a new technique for a sampling ECAL, in which an estimate of the number of particles in the shower is used as the measure of the shower energy, rather than the energy deposited. Clearly, these quantities are strong correlated, as each charged particle in the shower will deposit energy in the sensitive layer. However, the energy deposited depends on the speed and angle of the charge particle and also has fluctuations around the average deposit, as described by the Landau function [10]. Hence, it would be expected that the energy deposited would have a larger spread for any given shower than the number of particles. Therefore, an ECAL which measures the number of particles would have an intrinsically better resolution.

In the rest of this paper, Section 2 presents the fundamental properties of EM showers relevant to the study. Section 3 expands on the binary readout ECAL requirements, while Section 4 gives the expected shower resolution performance of a binary ECAL.

2. Basic studies

In this study, photon-induced EM showers are simulated using the GEANT4 program [11]. The nominal ECAL geometry used has 30 layers of 500 μm thick silicon sensors, with 0.6 radiation lengths (X_0) of tungsten in front of each of the first 20 layers and $1.2X_0$ in front of each of the last 10 layers. This geometry is typical of the designs being considered [8, 9]. To allow for the difference in tungsten thickness, the information from the last 10 layers is weighted by a factor of two compared to the first 20 layers for all energy and resolution estimates presented later,

Each layer is simulated to have a 1 mm thick PCB between the tungsten and the silicon sensors, assumed to be required for the sensor readout. There is also an air gap of 1 mm between the sensors of one layer and the tungsten of the next. While this represents a very simplified geometry compared with a realistic ILC-type ECAL, the shower properties are mainly dominated by the tungsten thickness and spacing and these correspond to realistic values.

Shower simulation uses ILC physics list.

For the results shown in this section, no experimental effects have been included in the simulation. Specifically, the analogue energy deposits are assumed to be measured perfectly, with no resolution effects, while the number of charged particles is determined from the perfect simulation information as the number of separate particles emerging from the bac surface of each silicon layer. Also, there are no dead regions in the sensitive layers.

Typical shower event display.

The basic result is illustrated in figure 1 which shows the distribution of the energy deposited and the number of charged particles for various incident photon energies. It is clear than the spread in the deposited energy is larger than than in the number of charged particles, for all photon energies.

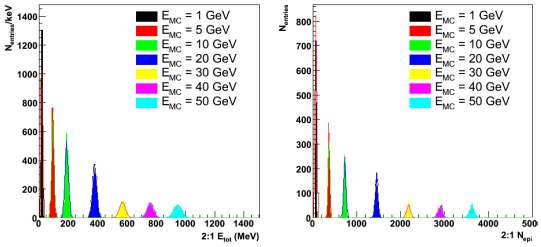

Figure 1: *Comparison of the distributions of the quantity measuring shower energy using (left) the energy deposited in the sensitive layers and (right) the number of charged particles crossing the sensitive layers. Results for a range of incident photon energies from 1 to 50 GeV are shown.*

This supports the basic contention that the number of charged particles is an intrinsically better measure of the shower energy than the deposited energy. Figure 2 shows the average value of each measure as a function of photon energy and shows both estimates demonstrate good linearity.

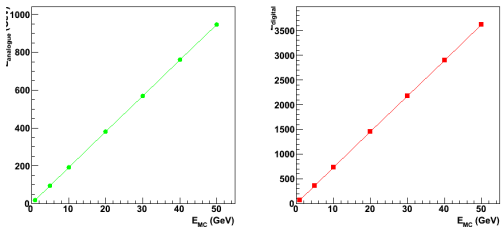

Figure 2: *Comparison of the linearity as a function of the incident photon energy, when measuring shower energy using (left) the energy deposited in the sensitive layers and (right) the number of charged particles crossing the sensitive layers.*

Figure 3 shows the root mean square (RMS) of each measure as an estimate of the basic irreducible

resolution in the two cases. It is clear the number of charged particles gives a very significant improvement over the energy deposited as an estimator of the incident photon energy. Fitting these resolutions to a function of the form

$$\frac{\sigma_E}{E} = \frac{s}{\sqrt{E \text{ in GeV}}} \oplus c$$

give values for the stochastic terms s of 14.6% for the "analogue" (energy deposited) case and 9.5% for the "digital" (number of charged particles) case, and for the constant terms c of 1.0% and 0.8%, respectively. Hence, the analogue case is degraded by a factor of around 1.5 compared to the digital case.

The above is for an ECAL without detector effects such as noise, dead areas, etc. It is known that a realistic analogue ECAL with low noise electronics can approach the intrinsic resolution for the analogue case [14]. The purpose of the study reported in the rest of the paper paper is to estimate the resolution of a realistic binary ECAL and compare it with the intrinsic resolution shown above.

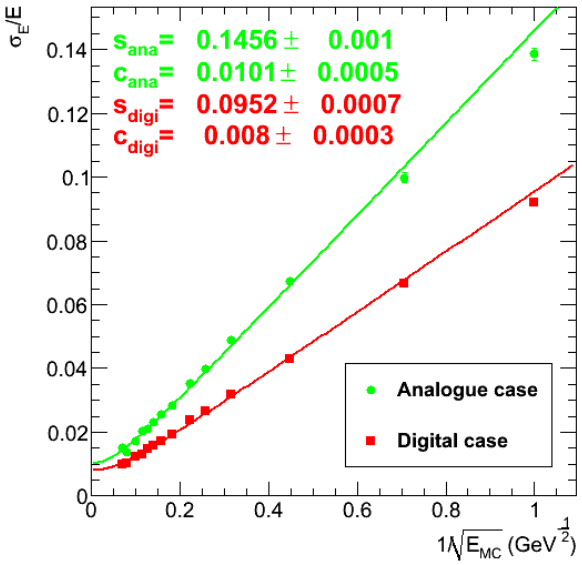

Figure 3: *Comparison of the resolution dependence on the incident photon energy, when measuring shower energy using (green) the energy deposited in the sensitive layers and (red) the number of charged particles crossing the sensitive layers. The lines show the results of the fits to the data points, as described in the text.*

3. Requirements

The results shown in the previous section motivate the development of an ECAL which is capable of estimating the number of charged particles in a shower. The method considered here is to propose an ECAL with binary readout, such that each pixel of the calorimeter gives a yes/no result to the presence of a charged particle. Any charged particle gives an average energy deposit which has a universal minimum at a particular particle velocity and for normal incidence. Any other speed or incident angle gives a larger mean deposit, so a threshold set below the minimum ionising particle (MIP) level, allowing also for the Landau spread, should be efficient for detecting all charged particles.

An ECAL designed to deliver good PFA performance will also need to be compact, minimising any gaps between the converter layers. This keeps the transverse spread of the EM showers small, measured by the effective Molière radius, as this helps separate particles close to each other in jets. Hence, the sensitive layers have to be as thin as possible compared to the converter thicknesses. For example, tungsten has a radiation length of $X_0 = 3.5\,\text{mm}$. Most ILC ECAL designs [8, 9] have only $\sim 0.5X_0$ in each of the first few layers, which therefore corresponds to $\sim 2\,\text{mm}$ of tungsten. Hence, sensitive detectors based on thin silicon sensors seem a sensible choice.

Implement as CMOS sensor. Epitaxial layer is sensitive area [**?**].

3.1. Pixel size

To give an accurate estimate, a sensor for counting charged particles would need to have a low probability of two charged particles crossing the same pixel. The density of charged particles per event, in the layer at which the density is a maximum, for 100 GeV EM showers is shown in figure 4. This simulation uses the nominal geometry described in Section 1. The peak value corresponds to 70 charged particles per mm^2; this would therefore require a pixel size significantly smaller than $0.014\,\text{mm}^2$. The sensor discussed in the rest of this paper is assumed to have a pixel size of $0.0025\,\text{mm}^2$, implemented as a square pixel of size $50 \times 50\,\mu\text{m}^2$.

This pixel size is two orders of magnitude smaller than any of the analogue pad ECALs being considered for the ILC [8, 9] and will be more than sufficient to allow PFA separation of particles. The size of the ECALs assumed in the ILC detector studies

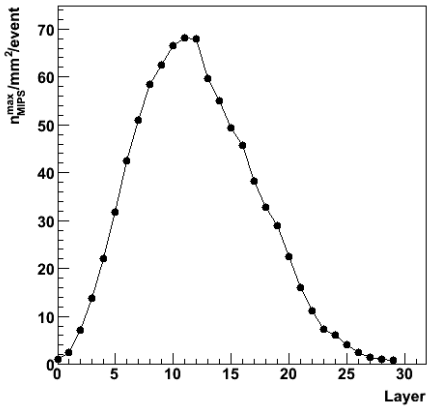

Figure 4: *Maximum density of charged particles per layer within 100 GeV EM showers, as a function of the layer in the shower.*

is large with a total sensor surface area of around $2000\,\mathrm{m}^2$. For $50\,\mu$m pixels, this would require a total of order 10^{12} pixels; hence this concept has been labelled the "tera-pixel" ECAL.

3.2. Noise

The ILC physics interaction rate for producing the high energy events of interest will be low; less than one per bunch train [2]. There will be significant levels of background from the ILC machine itself, as well as low energy physics events. However, with such a large number of pixels in a binary ECAL, then the overall hit rate will be dominated by the rate of noise. Assuming a threshold of around five times the noise, then the noise rate will be $\sim 10^{-6}$ per pixel per bunch crossing.

Size of typical shower times 30 layers to estimate number of pixel hits. Use previous plots to give number of particles.

3.3. Charge diffusion

3.4. Dead areas

3.5. Sensor assumptions

Assume: noise per pixel is 50 eV, charge spread is given by deep p-well [16], the sensor sensitive layer is $12\,\mu$m thick and the layer has an average dead area of 10%.

These are varied from 25 eV to 75 eV, zero charge diffusion to no deep p-well diffusion, $6\,\mu$m to $12\,\mu$m and 5% to 15%, respectively.

4. Physics performance

Given the results shown in the previous sections, it is possible to simulate the performance of a full scale binary ECAL. This study was done with the same sampling geometry as discussed in Section 3. These results supercede those presented previously [13].

4.1. Simulation

The underlying EM shower simulation used was based on the GEANT4 programme [11]. This simulation has been used extensively and in particular has been checked to high accuracy in an analogue silicon-tungsten sampling ECAL by the CALICE collaboration [14]. However, this ECAL had a pad granularity of $1 \times 1\,\mathrm{cm}^2$ and it is not known if the shower simulation is accurate at the much smaller granularities relevant for the binary ECAL simulation.

The energy deposited within each pixel was recorded on a grid of $5 \times 5\,\mu\mathrm{m}^2$ subpixels. These corresponded to squares formed with the 21 simulation points described in Section **??** at the corners. Within each subpixel, the energy deposited by all the particles in the event was summed. The simulation used units of the deposited energy throughout, so the plots below are in terms of these units.

Following the completion of the shower simulation, then this energy was shared between the hit pixel and the eight surrounding nearest neighbour pixels according to fractions determined from the charge diffusion simulation. The energy per pixel was then smeared by applying Gaussian noise and a threshold was applied to each pixel. For pixels with no energy (whether from the original shower or due to diffusion), then hits were added to random pixels with a rate corresponding to the noise and threshold values chosen. The effect of dead area was included by removing any hits in the inactive areas following the simulation process. The spectra of energies in each pixel at each stage of this process are shown in figure 5.

A nominal noise value of 120 eV was used; this corresponds to the low end of the noise distribution observed but is a realistic target for a future sensor. For a single MIP at normal incidence, the resulting efficiency for generating at least one hit when passing through a layer is shown in figure 6 as a function of the threshold applied. This should be compared with figure **??**, for which the calibration of TU means the range of the threshold axis

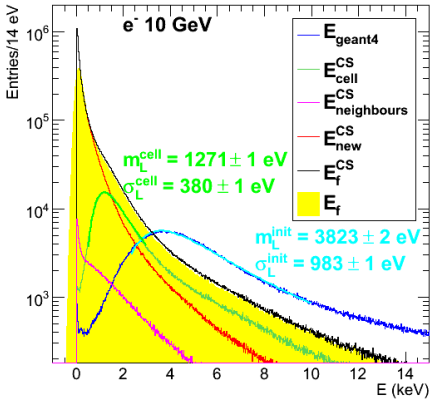

Figure 5: *Spectra of energy in each pixel at various stages of the sensor simulation. The spectra correspond to the original deposited energy (dark blue), the energy in the hit pixel after charge diffusion (green), noise in neighbouring pixels which were not hit (pink), the energy in the neighbouring pixels due to charge diffusion (red), and the total (black). The yellow histogram corresponds to the total smeared by the noise.*

shown in that figure corresponds to 9 keV, twice the range of figure 6. Both show a rise of around a factor of five in the range 1 keV to 4 keV, so giving some confidence that the simulation is reasonably reproducing the sensor performance.

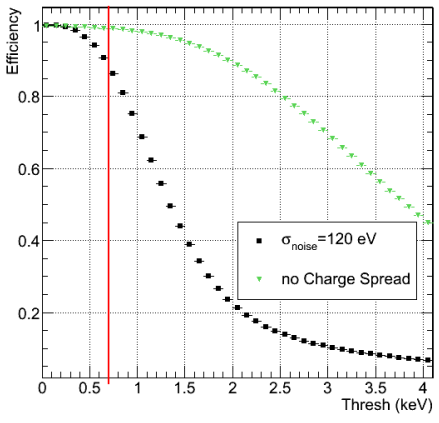

Figure 6: *Simulated of the efficiency for obtaining at least one hit from a MIP at normal incidence, as a function of the threshold. The squares correspond to the full simulation and the inverted triangle to a simulation with no charge diffusion. The vertical line indicates a typical threshold which would be used.*

4.2. MIP counting

Due to the charge diffusion between neighbouring pixels, it is possible for a single simulated MIP passing through a layer to result in anything from zero to nine hit pixels, depending on position, noise level and threshold. Hence, simply using the number of hit pixels as an estimate of the number of MIPs incurs a large error from this fluctuation. By clustering the neighbouring pixels and counting clusters rather than hits, it is possible to remove most of the effect of such fluctuations and so get a better estimate of the number of MIPs. This clustering is called "MIP counting" here.

A simple MIP counting algorithm was used for the following results. The pixels were grouped into isolated clusters, which were defined to be contiguous clusters of hit pixels with no further hits in any of the nearest neighbouring pixels. If the cluster contained no hit pixels for which all eight nearest neighbours also were hit, then the cluster was counted as one MIP. If one or more hit pixels had all eight nearest neighbours also hit, then the cluster was counted as having a number of MIPS equal to the number of such completely surrounded pixels. Clearly, this algorithm is not unique and is unlikely to be the best possible for this purpose. However, the optimisation depends on details of the EM shower behaviour at very fine granularity. These details have yet to be verified with real data and so finding the best MIP counting method cannot be done with any degree of realism at this stage.

4.3. Electromagnetic shower resolution

Using the MIP counting algorithm decribed above, the resulting EM shower resolution predicted by the simulation is shown in figure 7. It is seen that the resolution of the binary ECAL modelled here is degraded significantly with respect to the ideal digital case of perfect MIP counting. The stochastic term is increased from 9.5% to 13.0%, around 35% higher. However, note the binary ECAL is still predicted to have a better resolution than the ideal analogue ECAL which uses the same sampling fraction.

The various effects included in the simulation can be varied to observe their individual contributions to this degradation. For the following studies, an incident photon energy of 10 GeV was used, for which the value of σ_E/E is 3.2% for the ideal binary ECAL and 4.5% with the full simulation.

The effect of the deep P-well implant on the sensor is shown in figure 8. It is seen that for a sensor

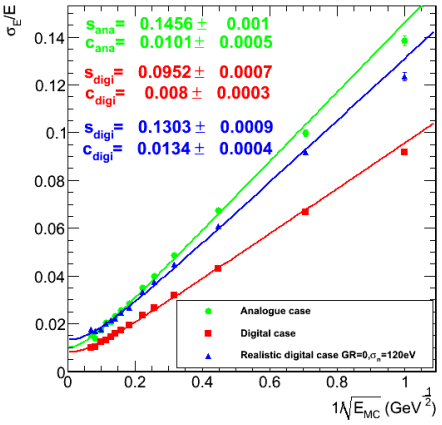

Figure 7: *Comparison of the resolution dependence on the incident photon energy. The red and green lines are the ideal cases, as shown in figure* **??**. *The blue line shows the result for a realistic binary ECAL after the full sensor simulation described in the text, including MIP counting.*

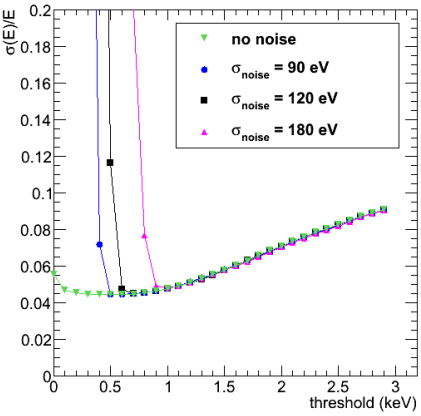

Figure 9: *Resolution for 10 GeV photons with simulated noise equivalent to 90 eV (cirles), 120 eV (squares) and 180 eV (triangles) energy deposited, as a function of the applied threshold. These correspond to the expected, best observed and average values of the sensor, respectively. Also shown is the resolution in the absence of noise (inverted triangles).*

with no deep P-well, the loss of charge to the unprotected N-well circuit diodes causes a very significant degradation of the resolution from 4.5% to 8.1%, more than doubling the ideal value and making the performance much worse than the ideal analogue ECAL.

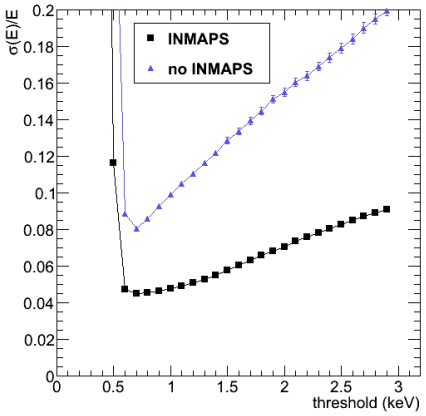

Figure 8: *Resolution for 10 GeV photons with (squares) and without (triangles) the deep P-well implant, as a function of the applied threshold.*

The effect of the noise is shown in figure 9. Noise affects the resolution through adding isolated hits which are counted as MIPs. While a correction can be made for the average number, these fake MIPs increase the resolution error due to the statistical fluctuation on the number of noise hits. The number of hits depends very strongly on threshold but, for high enough thresholds, the effect of the noise can be made small. Since the threshold can be chosen at will given a particular noise level, then by adjusting the threshold, the increase in resolution due to the noise can be reduced. The figure shows that higher noise gives an optimal resolution at a higher thresholds but that the resulting resolution degrades only slightly compared to the case with no noise. Note, the wide minimum for the case with no noise; 90 eV noise gives the same resolution as no noise, so indicating the level as which the noise becomes negligible. The optimal thresholds for the three noise values shown were found to be 0.5 keV for 90 eV noise, 0.7 keV for 120 eV noise and 1.0 keV for 180 eV noise. The resulting resolutions were 4.4%, 4.5% and 4.8%, respectively. Hence, the noise contribution to the degradation from the ideal resolution of 3.2% is small.

The effect of the dead area is shown in figure 10. It is seen that the effect of the SRAM memory dead area is to increase the resolution from 4.3% to 4.5%, again a small effect. By design, the dead area due to the on-sensor memory is spread out across the sensor. The EM showers have a width determined by the Molière radius of 9 mm and the memory dead areas are spaced out by 2.4 mm. This means every shower loses approximately the same fraction of hits

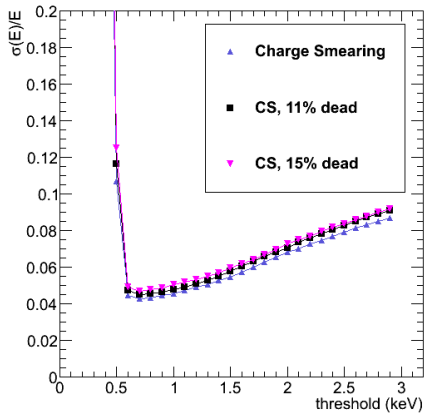

Figure 10: *Resolution for 10 GeV photons with dead area equivalent to 11% (squares) and 15% (inverted triangles), as a function of the applied threshold. These correspond to the on-sensor memory area and an estimate of the total dead area in a full-scale ECAL including edge effects around the sensor. Also shown is the resolution for a sensor with no inactive areas (triangles).*

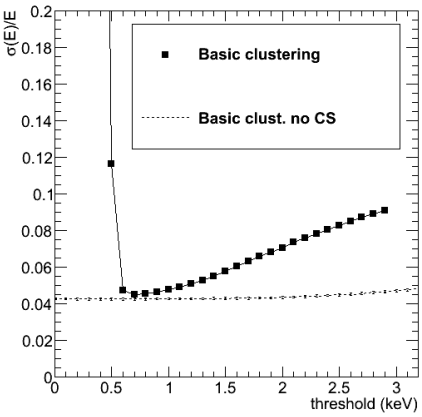

Figure 11: *Resolution for 10 GeV photons with (squares) and without (dashed line) charge diffusion, as a function of the applied threshold.*

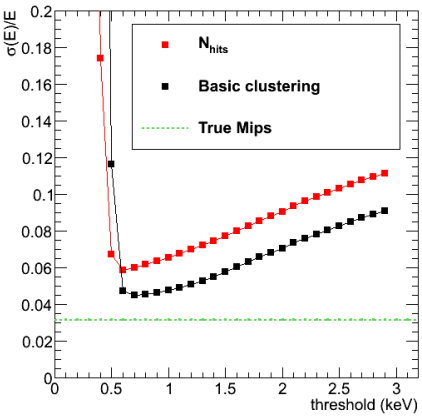

Figure 12: *Resolution for 10 GeV photons with no MIP counting (red) and with the simple MIP counting algorithm (black) as described in the text, as a function of the applied threshold. The horizontal line (green) shows the resolution obtained with an ideal MIP count.*

and so the resolution degrades by only the statistical fluctation on the number, not due to a variation in the mean number as a function of the impact position of the incident particle. Although somewhat uncertain, an estimate of the effect of extra dead area around the periphery of the sensor, and in gaps between sensors, for a realistic-sized sensor has been made. This may contribute a further 4% of dead area. The effect of this has also been modelled and is shown in figure 10 to give a very small contribution.

The effect of the charge diffusion is shown in figure 11. Although it is not physically possible to turn off the charge diffusion in the sensor, it is interesting to see how the charge diffusion affects the resolution. The figure shows the the resolution with and without simulating charge diffusion. The amount of charge per hit pixel is around three or four times higher on average without charge diffusion and so the effect of the threshold cut in the range considered is much smaller. However, at the optimal threshold, the resolutions with and without charge diffusion are very similar at 4.3% and 4.5%. Hence, the crosstalk from charge diffusion has a small effect for a binary ECAL application.

The effect of the MIP counting is shown in figure 12. The figure shows that using a naive hit count to estimate the number of MIPs gives a very large resolution, namely 5.9% compared with the 4.5% using a MIP counting algorithm, so using such an algorithm is essential to get good performance. However, the algorithm used does not bring the resolution down close to the ideal case value of 3.2%; there is still a significant difference between the ideal and realistic cases which is bigger than any of the effects previously considered.

Hence, the dominant contribution to the degradation of the resolution, even in the absence of noise, dead area and charge diffusion, is due to the confusion of interpreting the observed hits in terms of numbers of MIPs. It is clear that a major

study of MIP counting algorithms will be needed to find the limit of this approach. However, as stated above, the details of such an optimising MIP counting algorithm are likely to depend heavily on the details of EM showers. In particular, they will be sensitive to the core hit density in each layer and potentially to correlations between layers. As stated above, the GEANT4 shower simulation has not been verified at the very fine granularities relevant for these studies. Hence, it is essential to get real experimental data on showers at these granularities in order to know the real limits of the binary ECAL approach.

5. Further studies

5.1. Dependence on transverse radius

5.2. Weighting of hits

6. Conclusions

We have presented a study of a novel concept for sampling electromagnetic calorimetry; namely a calorimeter with binary readout. This requires very fine granularity and a high level of sensor integration to handle the very large number of pixels which are required.

The overall performance of a simulated full scale binary ECAL based on the test sensor results has been shown to give a better resolution for electromagnetic showers than an equivalent analogue readout ECAL. The dominating issue for the resolution is the algorithm for counting charged particles given the pattern of pixel hits observed. This is sensitive to the shower core density. The simulation has not been verified at this fine granularity required for a binary ECAL and so there is some uncertainty. Hence, this will require real data from EM showers at very fine granularity to understand the limiting resolution of a binary ECAL.

7. Acknowledgements

This work was funded in part through a grant from the Science and Technology Facilities Council (STFC), United Kingdom.

References

[1] "International Linear Collider Reference Design Report," (2007) `http://www.linearcollider.org/rdr`.

[2] "International Linear Collider Reference Design Report Volume 2: Physics at the ILC," ed A. Djouadi *et al.*, (2007) `http://www.linearcollider.org/rdr`.

[3] "TESLA TDR Part III: Physics at an e^+e^- Linear Collider," ed. R.-D. Heuer *et al.*, DESY 2001-011 (2001).

[4] CALICE Collaboration, `http://polywww.in2p3.fr/flc/calice.html`. NEW WEBSITE?

[5] M. A. Thomson, "Particle flow calorimetry at the ILC," Proceedings of Hadronic Shower Simulations Workshop, Batavia, Illinois (2006), AIP Conf. Proc. **896** (2007) 215; UPDATE?

[6] M. A. Thomson, "Progress with Particle Flow Calorimetry," Proceedings of 2007 International Linear Collider Workshop (LCWS07 and ILC07), Hamburg, Germany (2007), arXiv:0709.1360. UPDATE?

[7] J. E. Brau *et al.*, "Calorimetry for the NLC detector," Proceedings of the 1996 DPF/DPB Summer Study on New Directions in High-energy Physics, Snowmass, Colorado (1996) eConf C960625 DET077.

[8] SiD Detector Concept, `http://silicondetector.org/`. UPDATE TO TDR.

[9] ILD Detector Concept, `http://www.ilcild.org/`. UPDATE TO TDR.

[10] Landau shape ref.

[11] GEANT4 Collaboration, S. Agostinelli *et al.*, Nucl. Inst. Meth. **A506** (2003) 250. CHECK FOR UPDATE?

[12] Guinea Pig beam simulation, `http://www-sldnt.slac.stanford.edu/nlc/programs/guinea_pig/gp_in`

[13] J. A. Ballin *et al.*, "A MAPS-based Digital Electromagnetic Calorimeter for the ILC," Proceedings of 2007 International Linear Collider Workshop (LCWS07 and ILC07), Hamburg, Germany (2007), arXiv:0709.1346.

[14] CALICE Collaboration, C. Carloganu *et al.*, "Calice Si-W EM Calorimeter: Preliminary Results of the Testbeams 2006," Proceedings of 2007 International Linear Collider Workshop (LCWS07 and ILC07), Hamburg, Germany (2007), arXiv:0709.2516.

[15] J. A. Ballin *et al.*, "Design and performance of a CMOS test sensor for a binary readout electromagnetic calorimeter," Submitted to IEEE/TNS.

[16] J. A. Ballin *et al.*, "Monolithic Active Pixel Sensors (MAPS) in a quadruple well technology for nearly 100% fill factor and full CMOS pixels," to be published in Sensors (2008), arXiv:0807.2920. UPDATE.